photonics

MDPI

Article

Numerical Aperture-Dependent Spatial Scaling of Plasma Channels in HPHT Diamond

Yulia Gulina *, Jiaqi Zhu, George Krasin, Evgeny Kuzmin and Sergey Kudryashov

Lebedev Physical Institute, Moscow 119991, Russia; ch.czyaci@lebedev.ru (J.Z.); krasingk@lebedev.ru (G.K.); e.kuzmin@lebedev.ru (E.K.); kudryashovsi@lebedev.ru (S.K.)
* Correspondence: gulinays@lebedev.ru

Abstract: The investigation of plasma channels induced by focused ultra-short 1030-nm laser pulses in bulk of synthetic High Pressure High Temperature (HPHT) diamond revealed strong dependence of their spatial parameters on the used numerical aperture of the lens (NA = 0.15–0.45). It was shown that at weak focusing conditions it is possible to significantly increase the length of the plasma channel with a slight increase in pulse power, while tight focusing allows one to obtain more compact structures in the same range of used powers. Such a dependence paves the way to new possibilities in 3D processing of transparent dielectrics, allowing one, for example, to vary the spatial parameters of modified regions without changing the setup, but only by controlling the lens aperture, which seems very promising for industrial applications.

Keywords: ultrashort laser pulses; filamentation; nonlinear optical interaction; HPHT diamond; numerical aperture; plasma channels; photoluminescence

Citation: Gulina, Y.; Zhu, J.; Krasin, G.; Kuzmin, E.; Kudryashov, S. Numerical Aperture-Dependent Spatial Scaling of Plasma Channels in HPHT Diamond. *Photonics* **2023**, *10*, 1177. https://doi.org/10.3390/photonics10101177

Received: 14 September 2023
Revised: 12 October 2023
Accepted: 21 October 2023
Published: 23 October 2023

1. Introduction

The investigation of ultrafast light–matter interactions, particularly those involving femtosecond laser pulses and dielectric materials, has ushered in a new era of advancements across multiple scientific and technological domains. Ultra-short pulse lasers, characterized by short pulse durations and high peak intensities, offer unprecedented precision and control for laser-induced modifications of different materials in bulk, including metals, dielectrics, and semiconductors, and has found wide-ranging applications in precise microfabrication [1,2], optical communication [3], and biomedical imaging [4]. Femtosecond laser technology has found significant application in the fabrication of integrated photonic devices, involving the modification of transparent bulk materials to induce novel properties in the medium [5]. Several research groups have investigated the application of femtosecond laser (fs-laser) writing in diamond or diamond-like carbon materials. Notably, in [6] the authors successfully employed fs-laser technology to create parallel nanostructures approximately 300 μm in length on a single-crystalline diamond. Furthermore, employing femtosecond laser technology to fabricate microfluidic channels of different transparent materials in bulk represents a promising field. This approach holds potential for the development of diverse sensing devices on biocompatible materials, such as diamonds [7].

During the propagation of femtosecond laser pulses through a dielectric material, the electric field of these pulses induces a nonlinear polarization response within the material. This response leads to a change in the material's refractive index, which becomes intensity-dependent. Regions of the material where the laser beam has higher intensity exhibit a greater refractive index, resulting in a focusing effect and eventual collapse of the beam, known as catastrophic self-focusing, a third-order nonlinear optical phenomenon [8,9]. On the other hand, at increased laser intensities ionization occurs in the dielectric material, giving rise to plasma, a state consisting of free electrons and ions [10]. This phenomenon

can be described by the Drude model [11] or the plasma critical density condition. The generation of a plasma involves a local reduction in the refraction index causing the beam to diverge and counteract the self-focusing effect, resulting in plasma defocusing [12]. Plasma defocusing plays a crucial role in balancing the self-focusing effect, providing beam stability, and facilitating the formation of filament channels-extended areas with a consistently high energy density [13]. The process of filamentation directly affects energy deposition efficiency, which defines the trajectory and extent of laser-induced modifications. This complex nonlinear interaction leads to the formation of spatially confined regions with altered refractive indices known as "channels" caused by the light–matter interactions [14]. Investigation of the parameters of the nonlinear optical interaction that leads to the formation of plasma channels would allow one to manage its spatial characteristics, thus opening the possibility for more versatile in-bulk material modification, fabricating different micro- and nanostructures by changing the cross-section or the length and position of the modified region in transparent dielectrics. Such precise control of the modified region could be very promising for industrial applications.

Interaction between intense femtosecond lasers and transparent media have been intensively studied, but the main focus was on discovering material damage thresholds and their practical applications [15–17]. Another notable consequence of nonlinear laser–matter interaction is the formation of plasma channels. This process is influenced by various factors, including laser parameters (beam quality, pulse duration, wavelength, etc.) and medium properties (nonlinear refractive index (n_2), linear refractive index (n_0), and multiphoton absorption coefficient) [13,18,19]. Previous studies have examined the nonlinear optical effect of filamentation by analyzing plasma luminescent channels formed by ultrashort laser pulses of dielectric materials in bulk. Research conducted in [20] reported pulse-width dependent self-focusing critical powers for linearly and circularly polarized focused 515-nm and 1030-nm laser pulses with varying pulse widths in fused silica, fluorite, natural diamond, and synthetic diamond. Furthermore, a study [21] explored polarization-dependent filamentation by analyzing the luminescence of plasma channels generated in High Pressure High Temperature (HPHT) diamond under the influence of focused ultrashort laser pulses. However, the role of focusing geometry, specifically the numerical aperture (NA) of the focusing lens, remains relatively unexplored, providing an open field for investigation, particularly considering the variation in plasma density under tight and weak focusing conditions. When the focusing is not excessively tight, the medium tends to remain relatively uniform, resulting in less dense plasma generation [22]. Additionally, in [23], the phenomenon of micro-explosions induced by ultrafast laser pulses in transparent materials was examined, demonstrating that the focusing geometry plays a significant role in determining the expansion and propagation of shockwaves. In [24], it was demonstrated that tightly focused femtosecond laser pulses can induce optical breakdown and structural changes in glass, even at low pulse energies achievable without amplification. Examining the formation of filaments and associated refractive index changes using focusing lenses with different NAs, a study conducted in [25] observed that the length of the region exhibiting refractive index changes increased with decreasing NA. Investigating the intricacies of femtosecond pulse propagation in fused silica under weak focusing conditions, including the effects of self-focusing and defocusing due to the presence of a free electron plasma, ref. [26] shed light on the role of NA in controlling the interaction of femtosecond laser pulses with transparent materials. Emphasizing the influence of NA on supercontinuum generation and damage thresholds, ref. [27] confirmed bulk damage at all NA studied, with catastrophic damage occurring at high NA. Further exploration of the NA dependence of white-light continuum generation and material damage in different samples was conducted in [28]. As an independent linear optical parameter, NA plays a crucial role in controlling the interaction between femtosecond laser pulses and transparent materials, impacting the generation of supercontinuum and the occurrence of material damage. Through high-resolution three-dimensional simulations and analysis of filamentation under varying focusing conditions, it was revealed in [29]

that the filamentation process is influenced by the interplay between geometric focusing and the nonlinear Kerr effect. A transition from the linear focusing mechanism to the nonlinear focusing mechanism during filamentation in air, illustrating changes in physical equilibrium through the degree of focus, was proposed in [30,31]. Under high-NA conditions, the Kerr self-focusing effect becomes negligible compared to plasma defocusing and geometric focusing. Despite these findings, the impact of NA on filamentation threshold power remains largely unexplored, resulting in a knowledge gap regarding the dynamics of femtosecond laser propagation.

This research aims to investigate the relationship between numerical aperture and the filamentation process leading to the formation of plasma channels. The selection of suitable materials plays a crucial role in these nonlinear interactions. HPHT diamond, renowned for its exceptional thermal and optical properties, serves as an intriguing platform for studying ultrafast laser–material interactions. The impressive attributes of HPHT diamond, including its high thermal conductivity, wide bandgap, and robust optical nonlinearity [32], position it as an outstanding candidate for advancing our comprehension of ultra-short pulse propagation and filamentation phenomena. Such insights hold the potential to contribute to more effective and precise utilization of femtosecond laser technology.

2. Materials and Methods

The femtosecond fiber Yb^{+3} ion laser Satsuma (Amplitude Systemes, Pessac, France) with wavelength of 1030 nm was used as a source of linearly polarized radiation. The laser pulses were focused in bulk of a HPHT synthetic type IIA diamond with dimensions of 3 × 1.5 × 1.5 mm^3 using a quartz/fluorite microscope objective with numerical aperture NA = 0.55. The numerical aperture value was adjusted in the range NA = 0.15–0.45 (corresponding focal spot size with $1/e^2$ radius $w_0 \approx 2.2$–0.73 μm) by changing the size of the laser beam provided by means of a variable diaphragm mounted in front of the objective. The beam diameter was controlled using a CCD camera at $1/e^2$ intensity level. During the multi-pulse exposure of ultrashort pulses with a duration of ~300 fs, a repetition rate of ν = 100 kHz, and pulse energy range E = 40–350 nJ, the formation of extended luminous plasma channels was observed in the rear focal plane of the microscope objective. Based on Raman spectroscopy observations made using a Confotec MR520 (SOL instruments, Minsk, Belarus) microscope–spectrometer and optical microscopy, it was found that in the studied pulse energy range there were no modifications in the sample in the form of aggregation of vacancy centers, or damage in the form of graphitization. The 1030-nm ultrashort laser pulses only provided nonlinear interband photoexcitation of characteristic free-excitonic photoluminescence (PL) in the bulk of the sample [33]. Micro-images of these luminous plasma channels were captured at a right angle using a NA = 0.2 microscope objective and monochromatic CMOS-camera CS2100M-USB Quantalux (Thorlabs, Newton, NJ, USA) (see Figure 1a).

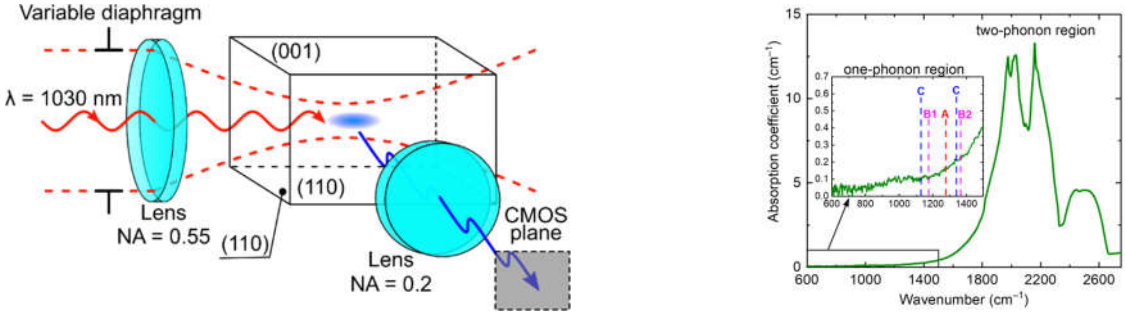

Figure 1. (**a**) Experimental scheme for registration of luminous plasma channels in the HPHT diamond. (**b**) Optical absorption spectrum of the sample; inset shows the mid-IR absorption spectra with the positions of the main optical defects marked.

The irradiation was focused in the bulk of the sample via (110) face at a normal angle and the images of the luminous channels were captured at a right angle via another (110) face. The optical absorption spectrum of the sample was obtained using an IR spectrometer VERTEX 70v (Bruker, Karlsruhe, Germany). The obtained spectral characteristics shown in Figure 1b demonstrate the absence of nitrogen impurity absorption bands (<1 ppm), and the inter-band electron-hole plasma photoexcitation presumably occurs in a pure carbon-carrier matrix [33]. Therefore, the analysis of luminous channels in such a sample paves the way to understanding the fundamental basis of nonlinear inter-band photoexcitation, being the initial stage of the filamentation and energy deposition processes in diamonds in general.

3. Experimental Results

3.1. Dimensional Parameters of Luminous Channels vs. NA

The micro-images of the luminous spatial channels induced by the ultrashort laser pulses are shown in Figure 2. Firstly, the focusing conditions were determined using a microscope objective with the aperture value NA = 0.2. The luminous channels appeared around the central position of the linear focus $z_f \approx 1300$ μm at pulse energies E ≥ 100 nJ. With a further increase in energy, channels began to asymmetrically elongate from the geometric focus towards the incident radiation (Figure 2a). This is due to the increase in the contribution of nonlinear effects to the process of in-bulk laser–matter interaction. When the pulse power exceeds the critical power of a certain threshold value, the filamentation process begins, which leads to a nonlinear broadening of the spectrum of passing pulses, which is clearly demonstrated in Figure 2b. The spectrum is symmetrical for pulses with a power of less than 0.5 MW, but with a further increase in power it widens, and side peaks appear in the red and blue regions, which indicates the presence of self-focusing and the formation of dense defocusing plasma resulting from photoionization [13,30,34–36]. At the same time, its central maximum shifts toward the blue region with increasing power, which is consistent with the results obtained in [37].

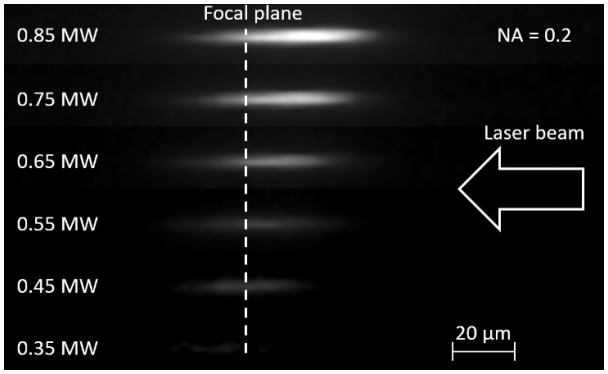

(**a**)

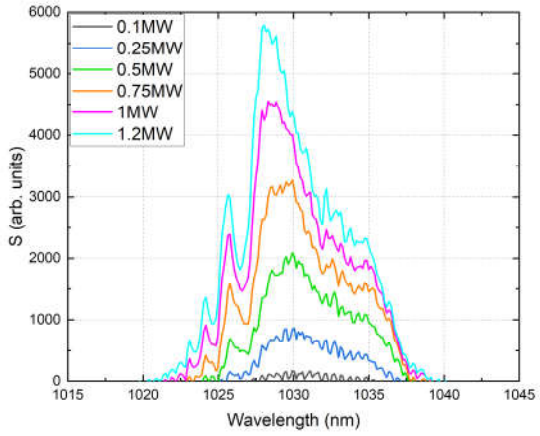

(**b**)

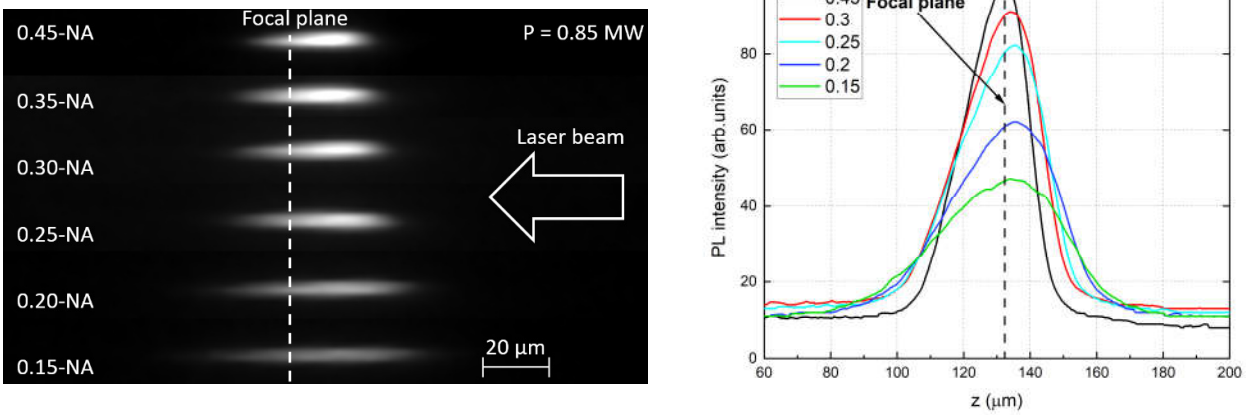

(**c**) (**d**)

Figure 2. (**a**) Micro-images of the luminous plasma channels for fixed NA = 0.2 focusing with varying peak pulse power P = 0.35–0.85 MW and (**c**) for fixed peak pulse power P = 0.85 MW and varying NA = 0.15–0.45. (**b**) Spectra of laser pulse transmitted through the sample at different incident pulse powers for NA = 0.2. (**d**) The cross-sections for a few selected luminous channels for peak power P = 0.85 MW.

The generation of plasma channels is caused by the combined effect of a number of nonlinear optical effects as well as focusing geometry. The intensity required to start the photoionization process leading to plasma formation can be achieved both due to nonlinear Kerr focusing and linear geometrical focusing. To study the effect of focusing conditions on the filamentation process, we analyzed plasma channels induced at a fixed peak pulse energy P = 0.85 MW while varying the numerical aperture from 0.45 to 0.15. The transition from long plasma channels for NA < 0.2 to a compact structure for tighter focusing conditions is clearly demonstrated in Figure 2c. As we decrease the focal spot size by using higher NA, the plasma channel length shortens, becoming a compact structure for tight focusing (NA = 0.45, $w_0 \approx 0.73$ μm). It can be also observed that for weak focusing, plasma creation begins sooner, before the geometrical focus, although the incident laser intensity is smaller for larger spot sizes (since the total peak power is kept constant) and luminous channels are elongated toward the upstream direction of the laser pulses with decreasing numerical aperture. This is due to the fact that self-focusing leads to a nonlinear shift in the focal position, and an increase in intensity in this area leads to the generation of dense luminous plasma before the geometric focal plane. This indicates that the nonlinear Kerr effect and self-focusing must play an important role in the regime with longer plasma channels. In contrast, for tighter focusing conditions, the position of the focus is very close to the geometrical focus, indicating a potentially smaller contribution of the nonlinear Kerr effect and domination of geometrical focusing. Thus, the luminous channel formed under tight focusing conditions has higher intensity and shorter length, while under weak focusing conditions, the medium remains relatively uniform and the generated plasma is not very dense, and the channel intensity is limited by nonlinear effects (multiphoton absorption and plasma defocusing) and its length is greater (Figure 2d).

The measured lengths of observed channels are presented in Figure 3a. The lengths varied from 5 to 120 μm, depending on the NA of the focusing lens and peak pulse power. As can be seen, the length enlarges nonlinearly with increasing pulse power, and for lower apertures the length of the channels is significantly longer than for high ones. This is clearly demonstrated in Figure 3b, where the dependence of the channel length on the numerical aperture is shown.

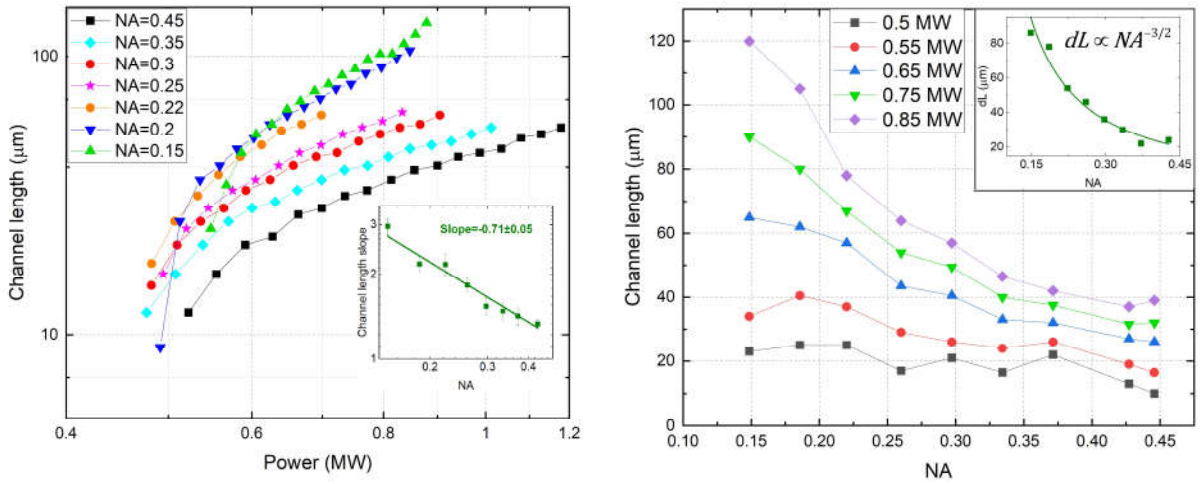

(**a**) (**b**)

Figure 3. Dependence of the luminous channel length on pulse power (**a**) and on NA (**b**). Luminous channel length error bars: 10%. *dL* in the inset shows the range of the channel length change.

The range of the channel length change nonlinearly decreases with the growth of the aperture as $dL \propto NA^{-3/2}$ and at low apertures it is several times greater than at high ones (see Figure 3b). That is, with weak focusing, it is possible to significantly increase the length of the plasma channel with a slight increase in pulse power, while with tight focusing, it is possible to obtain more compact structures in the same range of used powers.

3.2. Filamentation Threshold Power vs. NA

In our research, the onset of the filamentation process was identified as a visible asymmetric elongation of the luminous channels with increasing pulse power. This elongation is defined as the asymmetry in the length of the parts of the longitudinal section counted from the center of symmetry of the channel obtained at low power (see Figure 4a). Under such conditions, nonlinear effects do not affect the propagation of radiation and only geometrical focusing takes place. With an increase in laser power, the back part of the channel elongates linearly, due to the increase in the brightness of the focal area, so it is called the "linear part". The front part of the channel elongates due to combination of nonlinear effects and is called the "nonlinear part". The laser power at which nonlinear part exceeds linear part is the point where self-focusing starts working—filamentation threshold power. The accuracy with which this power threshold is determined depends mostly on instrumental error, that is the ability of the camera to detect correctly successive changes in the shape and position of the channel with the variation in laser power. Our estimations, based on camera resolution and the lens used, shows a total error of approximately 10%.

Experimental dependence of the filamentation threshold power acquired with different NAs is shown in Figure 4b.

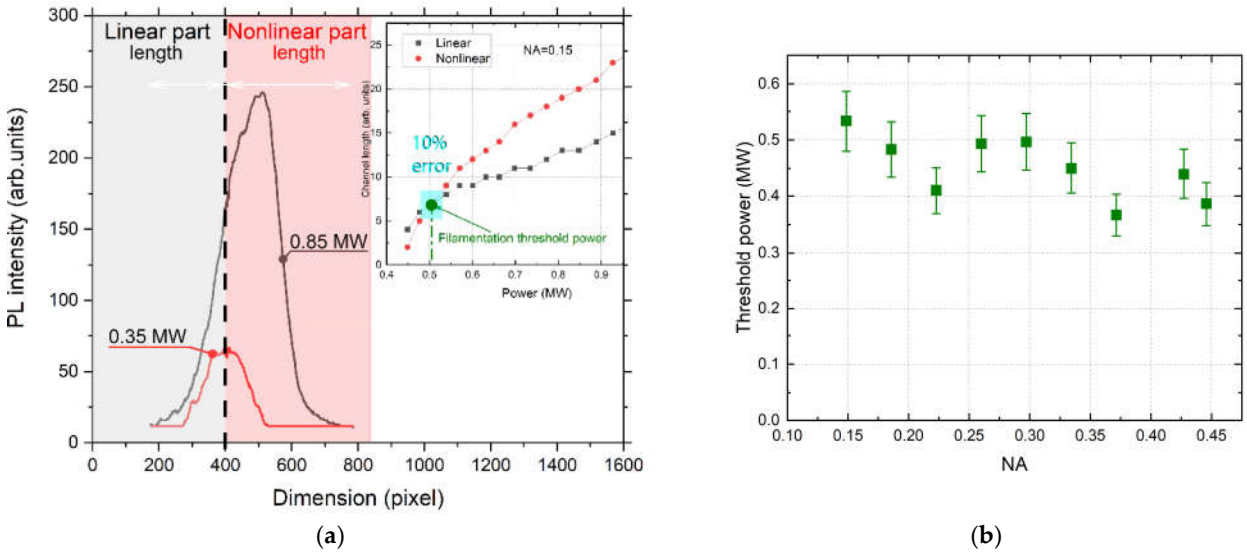

(**a**) (**b**)

Figure 4. (**a**) Dependence of the luminous channel lengths on the peak pulse power; (**b**) dependence of the filamentation threshold power on NA.

Self-focusing does not depend on intensity, but only on the peak power [11,31]; thus, the critical self-focusing threshold does not depend on the focusing geometry determined by the aperture and is the same for tight and weak external focusing. However, the contribution of plasma defocusing to filament formation strongly depends on focusing conditions [29]. When using high-NA focusing, the plasma density required to balance the Kerr nonlinearity can be obtained at lower pulse energies. Thus, the threshold for the filamentation onset with tighter focusing conditions will be lower than with weak focusing: the filamentation threshold power is equal to $P_{th} \approx 0.55 \pm 0.05$ MW for NA = 0.15 and $P_{th} \approx 0.38 \pm 0.05$ MW for NA = 0.45.

3.3. PL Intensity vs. NA

It is known that bends in the slopes in the pump power-dependent stationary PL output can be identified as transition points between different characteristic regimes, apparently representing some features of ultrafast inter-band photoexcitation accompanying the dynamics of free charge carriers and the filamentation process [19,38,39]. The dependences of the peak PL intensity of the observed channels on the peak pulse power for different NAs are shown in Figure 5a. With weak focusing geometry, there is a bend in the dependencies observed in the region of 0.4–0.5 MW, which corresponds to the estimated value of the threshold power of the filamentation onset. In the pre-filamentation mode (Regime #1), the slope of the curves increases with the growth of the numerical aperture from 0.55 to 0.75, which happens due to the dominance of geometric linear focusing over nonlinear. However, at higher energies in the filamentation regime (Regime #2), an increase in the slope of the curves is observed, which is due to an increase in the intensity in the near-axial region caused by the Kerr nonlinearity. At the same time, the slope of all curves becomes the same and does not depend on the aperture, which indicates the predominance of non-linear focusing. It should be noted that there is almost no change in the slope for tight focusing NA = 0.45; this is probably due to the fact that geometric focusing is the determining factor in the entire studied energy range.

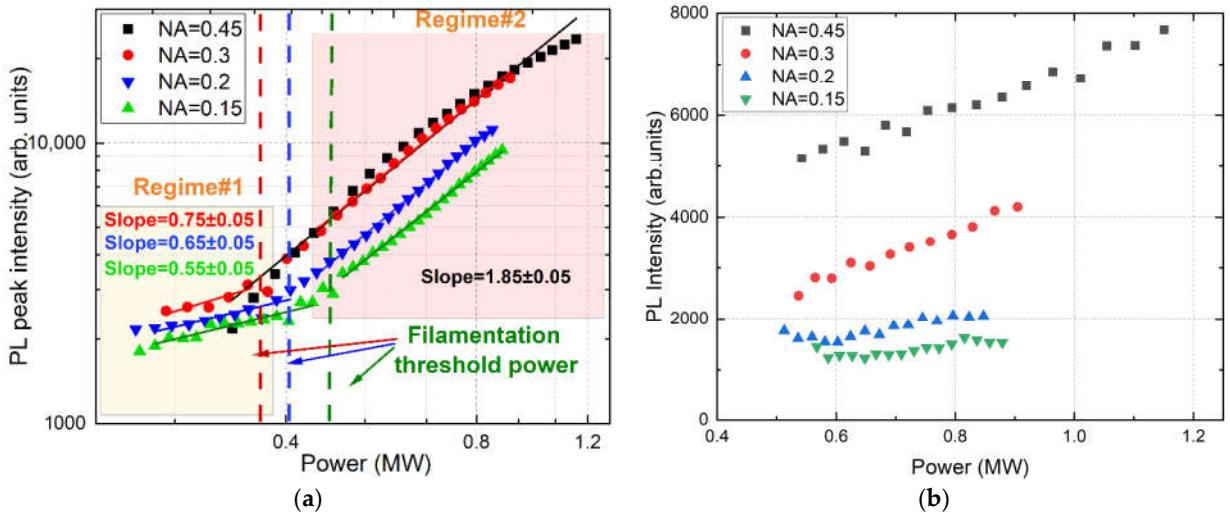

Figure 5. Dependence of the PL peak intensity (**a**) and integrated PL intensity (**b**) on pulse power. PL intensity error bars: 10%.

With an increase in the pulse energy, the size of the photoluminescence region begins to increase, therefore, to assess the effect of pulse power and NA on the PL due to nonlinear effects, we normalized the dependences of the integrated PL intensity on the channel length (Figure 5b). It was found that for weak focusing conditions (NA = 0.15, 0.2), with an increase in the intensity of ultrashort laser pulses in the registered plasma channels, there is almost no increase in the PL yield and that pulse energy goes into the channel elongation, which is in good agreement with the well-known fact about intensity clamping in the filamentation process [40,41]. However, with tight focusing (NA > 0.3), there is a monotonous increase in the PL yield with increasing peak pulse power, which is due to the dominance of geometric linear focusing and the deposition of laser energy in the limited focal area accompanied by the generation of dense luminous plasma.

4. Discussion

The observed luminous plasma channels were the result of a set of nonlinear optical effects accompanying the filamentation process. As noted above, in the studied pulse energy range there was no aggregation of vacancy centers or graphitization in the bulk of the sample. In this case, the modification of the material was expressed in a local change in the refractive index and was of a temporary nature, due to the relaxation time of free carrier charges generated during the photoionization of the medium. The intensity-dependent refractive index of the modified region due to the Kerr nonlinearity can be represented as:

$$n(I) = n_0 + n_2 I, \quad (1)$$

where n_0 is the linear refractive index of the medium, n_2 is the nonlinear refractive index of the medium, and I is the intensity of laser radiation.

The filamentation process is initiated by self-focusing of the laser pulse, which occurs when the input laser power exceeds the critical power and leads to the nonlinear shift of the focal area position towards the laser radiation. In the general case in which the beam has arbitrary power and arbitrary beam-waist position, the distance from the entrance face of the sample to the position of the self-focus, taking into account the intensity-dependent refractive index, can be estimated by the refined expression [34]:

$$z_{sf} = \frac{\frac{1}{2}k(I)w^2}{\left(\frac{P}{P_{th}}-1\right)^{\frac{1}{2}} + 2z_f/k(I)w_0^2}, \quad (2)$$

where $k(I) = 2\pi n(I)_0/\lambda$ is the intensity-dependent wavenumber in the medium, and w is the $1/e^2$ beam radius at the entrance face. Using the threshold value of the filamentation onset P_{th} determined from the experimental data, the dependencies of nonlinear focal shift $df = z_f - z_{sf}$ on the pulse peak power were calculated (Figure 6a, solid lines). For comparison, experimental shifts were also determined (symbols).

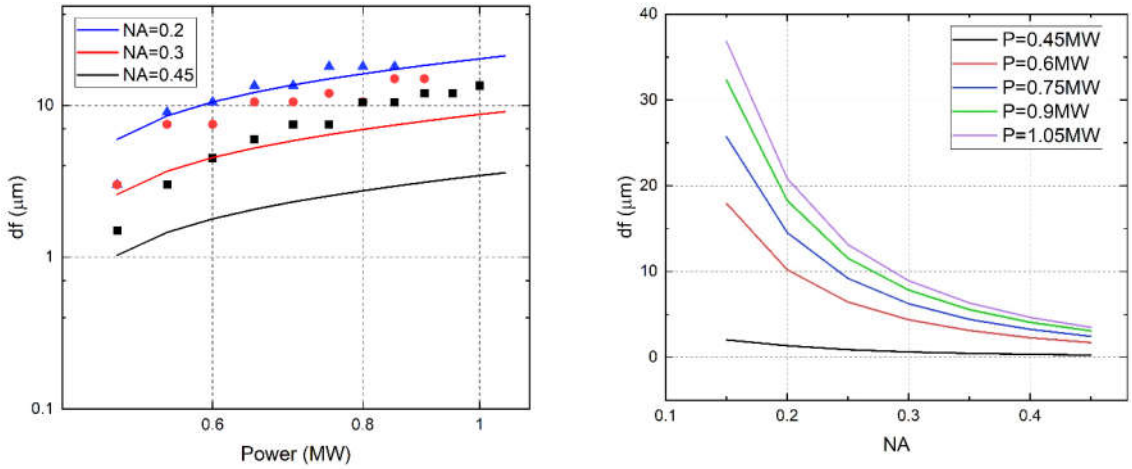

(**a**) (**b**)

Figure 6. Dependence of nonlinear focal shift on peak pulse power (**a**) and on NA (**b**). Focal shift error bars: 10%.

It can be seen that at weak focusing conditions (NA = 0.2) there is good agreement between theoretical and experimental focal shifts, but at higher apertures the theoretical calculations are several times lower than the experimental ones. Moreover, with an increase in NA, the discrepancy in shifts also increases. This effect may be associated with plasma shielding. The dense plasma generated in the focal area partially absorbs laser irradiation and reflects it towards the laser beam, and only a fraction of the irradiation passes through this region. This effect simultaneously leads to a decrease in the length of the "linear" part (since it becomes dimmer than it could be) and to a lengthening of the "nonlinear" part (since the reflected photons fly towards the laser beam). This ultimately leads to an underestimation of the focal shift in the calculation model, which is based only on the effect of Kerr self-focusing and beam diffraction and does not take plasma impact into account. Moreover, with an increase in NA the plasma becomes denser and the fraction of the transmitted energy decreases, while the fraction of the absorbed and reflected energy increases. This leads to an increase in the discrepancy between experimental focal shifts and theoretical calculations under tighter focusing conditions.

In Figure 6b, the theoretically calculated dependences of the nonlinear focal shift on NA are presented. It can be noticed that at higher NAs focal shift is less subject to change and remains almost stable as power increases, whereas at low NA there is an increase by several times. This opens up possibilities for controlling such spatial parameters as the size and the position of the modified regions by varying the aperture of the focusing optics in a limited range of energies.

5. Conclusions

In conclusion, laser irradiation of HPHT diamond with ultra-short 1030 nm pulses at different NAs revealed a strong dependence of the size, shape, and position of the modified region on the used NA of the lens. Such a dependence opens up another degree of freedom in 3D processing in transparent dielectrics, allowing one to realize spatial scaling

of modified areas, for example, to vary the cross-section of the waveguide, without changing the recording setup, but only by controlling the lens aperture, which seems very promising for industrial applications.

Author Contributions: Conceptualization, Y.G. and S.K.; methodology, Y.G., G.K. and E.K; software, Y.G., G.K. and E.K.; validation, Y.G. and S.K.; formal analysis, J.Z., G.K. and E.K.; investigation, Y.G. and G.K.; resources, S.K.; data curation, G.K. and E.K.; writing—original draft preparation, Y.G. and J.Z.; writing—review and editing, Y.G., G.K., E.K. and S.K.; visualization, Y. G., G.K. and E.K.; supervision, S.K.; project administration, S.K.; funding acquisition, S.K. All authors have read and agreed to the published version of the manuscript.

Funding: The study is funded by the grant of Russian Science Foundation (project № 21-79-30063); https://rscf.ru/en/project/21-79-30063/.

Institutional Review Board Statement: Not applicable.

Informed Consent Statement: Not applicable.

Data Availability Statement: The data presented in this study are available on request from the corresponding author.

Conflicts of Interest: The authors declare no conflicts of interest.

References

1. Sugioka, K.; Cheng, Y. Ultrafast Lasers—Reliable Tools for Advanced Materials Processing. *Light Sci. Appl.* **2014**, *3*, e149–e149. https://doi.org/10.1038/lsa.2014.30.
2. Kudryashov, S.; Nastulyavichus, A.; Krasin, G.; Khamidullin, K.; Boldyrev, K.; Kirilenko, D.; Yachmenev, A.; Ponomarev, D.; Komandin, G.; Lebedev, S.; et al. CMOS-compatible direct laser writing of sulfur-ultrahyperdoped silicon: Breakthrough prerequisite for UV-THz optoelectronic nano/microintegration. *Opt. Laser Technol.* **2023**, *158*, 108873. https://doi.org/10.1016/j.optlastec.2022.108873.
3. Temprana, E.; Myslivets, E.; Kuo, B.-P.; Liu, L.; Ataie, V.; Alic, N.; Radic, S. Overcoming Kerr-Induced Capacity Limit in Optical Fiber Transmission. *Science* **2015**, *348*, 1445–1448. https://doi.org/10.1126/science.aab1781.
4. Horton, N.G.; Wang, K.; Kobat, D.; Clark, C.G.; Wise, F.W.; Schaffer, C.B.; Xu, C. In Vivo Three-Photon Microscopy of Subcortical Structures within an Intact Mouse Brain. *Nat. Photonics* **2013**, *7*, 205–209. https://doi.org/10.1364/cleo_si.2012.cth5c.4.
5. Della Valle, G.; Osellame, R.; Laporta, P. Micromachining of photonic devices by femtosecond laser pulses. *J. Opt. A Pure Appl. Opt.* **2008**, *11*, 013001. https://doi.org/10.1088/1464-4258/11/1/013001
6. Shinoda, M.; Gattass, R.R.; Mazur, E. Femtosecond laser-induced formation of nanometer-width grooves on synthetic single-crystal diamond surfaces. *J. Appl. Phys.* **2009**, *105*, 053102. https://doi.org/10.1063/1.3079512
7. Su, S.; Li, J.; Lee, G.C.B.; Sugden, K.; Webb, D.; Ye, H. Femtosecond laser-induced microstructures on diamond for microfluidic sensing device applications. *Appl. Phys. Lett.* **2013**, *102*, 231913. https://doi.org/10.1063/1.4811170
8. Chekalin, S.V.; Kandidov, V.P. From Self-Focusing Light Beams to Femtosecond Laser Pulse Filamentation. *Phys. Uspekhi* **2013**, *56*, 123. https://doi.org/10.3367/ufne.0183.201302b.0133.
9. Marburger, J.H. Self-Focusing: Theory. *Prog. Quantum Electron.* **1975**, *4*, 35–110. https://doi.org/10.1016/0079-6727(75)90003-8.
10. Mao, S.S.; Quéré, F.; Guizard, S.; Mao, X.; Russo, R.E.; Petite, G.; Martin, P. Dynamics of Femtosecond Laser Interactions with Dielectrics. *Appl. Phys. A* **2004**, *79*, 1695–1709. https://doi.org/10.1007/s00339-004-2684-0.
11. Mann, C.R. The Theory of Optics. By Paul Drude. Translated from the German by CR Mann and RA Millikan. New York, Longmans, Green & Co. 1902. Pp. Xxi+ 546. *Science* **1903**, *18*, 432–434. https://doi.org/10.1126/science.18.457.432.
12. Chen, F.F. *Introduction to Plasma Physics and Controlled Fusion*; Springer: Berlin/Heidelberg, Germany, 1984; Volume 1. https://doi.org/10.1007/978-3-319-22309-4_11.
13. Couairon, A.; Mysyrowicz, A. Femtosecond Filamentation in Transparent Media. *Phys. Rep.* **2007**, *441*, 47–189. https://doi.org/10.1016/j.physrep.2006.12.005.
14. Théberge, F.; Liu, W.; Simard, P.T.; Becker, A.; Chin, S.L. Plasma Density inside a Femtosecond Laser Filament in Air: Strong Dependence on External Focusing. *Phys. Rev. E* **2006**, *74*, 036406. https://doi.org/10.1103/physreve.74.036406.
15. Stuart, B.C.; Feit, M.D.; Herman, S.; Rubenchik, A.M.; Shore, B.W.; Perry, M.D. Nanosecond-to-Femtosecond Laser-Induced Breakdown in Dielectrics. *Phys. Rev. B* **1996**, *53*, 1749. https://doi.org/10.1103/physrevb.53.1749.
16. Neauport, J.; Lamaignere, L.; Bercegol, H.; Pilon, F.; Birolleau, J.-C. Polishing-Induced Contamination of Fused Silica Optics and Laser Induced Damage Density at 351 Nm. *Opt. Express* **2005**, *13*, 10163–10171. https://doi.org/10.1364/opex.13.010163.
17. Couairon, A.; Sudrie, L.; Franco, M.; Prade, B.; Mysyrowicz, A. Filamentation and damage in fused silica induced by tightly focused femtosecond laser pulses. *Phys. Rev. B* **2005**, *71*, 125435. https://doi.org/10.1103/PhysRevB.71.125435.
18. Gattass, R.R.; Mazur, E. Femtosecond Laser Micromachining in Transparent Materials. *Nat. Photonics* **2008**, *2*, 219–225. https://doi.org/10.1038/nphoton.2008.47.

19. Bergé, L.; Skupin, S.; Nuter, R.; Kasparian, J.; Wolf, J.-P. Ultrashort Filaments of Light in Loosely Ionized, Optically Transparent Media. *Rep. Prog. Phys.* **2007**, *70*, 1633. https://doi.org/10.1088/0034-4885/70/10/r03.
20. Kudryashov, S.I.; Danilov, P.A.; Kuzmin, E.V.; Gulina, Y.S.; Rupasov, A.E.; Krasin, G.K.; Zubarev, I.G.; Levchenko, A.O.; Kovalev, M.S.; Pakholchuk, P.P. Pulse-Width-Dependent Critical Power for Self-Focusing of Ultrashort Laser Pulses in Bulk Dielectrics. *Opt. Lett.* **2022**, *47*, 3487–3490. https://doi.org/10.1364/ol.462693.
21. Krasin, G.K.; Gulina, Y.S.; Kuzmin, E.V.; Martovitskii, V.P.; Kudryashov, S.I. Polarization-Sensitive Nonlinear Optical Interaction of Ultrashort Laser Pulses with HPHT Diamond. In *Photonics*; Multidisciplinary Digital Publishing Institute: Basel, Switzerland, 2023; Volume 10, p. 106. https://doi.org/10.3390/photonics10020106.
22. Dubietis, A.; Couairon, A. *Ultrafast Supercontinuum Generation in Transparent Solid-State Media*; Springer: Berlin/Heidelberg, Germany, 2019. https://doi.org/10.1007/978-3-030-14995-6.
23. Glezer, E.N.; Mazur, E. Ultrafast-Laser Driven Micro-Explosions in Transparent Materials. *Appl. Phys. Lett.* **1997**, *71*, 882–884. https://doi.org/10.1063/1.119677.
24. Schaffer, C.B.; Brodeur, A.; García, J.F.; Mazur, E. Micromachining Bulk Glass by Use of Femtosecond Laser Pulses with Nanojoule Energy. *Opt. Lett.* **2001**, *26*, 93–95. https://doi.org/10.1364/ol.26.000093.
25. Yamada, K.; Watanabe, W.; Toma, T.; Itoh, K.; Nishii, J. In Situ Observation of Photoinduced Refractive-Index Changes in Filaments Formed in Glasses by Femtosecond Laser Pulses. *Opt. Lett.* **2001**, *26*, 19–21. https://doi.org/10.1364/ol.26.000019.
26. Wu, A.Q.; Chowdhury, I.H.; Xu, X. Plasma Formation in Fused Silica Induced by Loosely Focused Femtosecond Laser Pulse. *Appl. Phys. Lett.* **2006**, *88*, 111502. https://doi.org/10.1063/1.2183361.
27. Ashcom, J.B.; Gattass, R.R.; Schaffer, C.B.; Mazur, E. Numerical Aperture Dependence of Damage and Supercontinuum Generation from Femtosecond Laser Pulses in Bulk Fused Silica. *JOSA B* **2006**, *23*, 2317–2322. https://doi.org/10.1364/josab.23.002317.
28. Poudel, M.P.; Chen, J. Nonlinear Optical Effects during Femtosecond Photodisruption. *Opt. Eng.* **2009**, *48*, 114302–114304. https://doi.org/10.1117/1.3264973.
29. Naseri, N.; Dupras, G.; Ramunno, L. Mechanism of Laser Induced Filamentation in Dielectrics. *Opt. Express* **2020**, *28*, 26977–26988. https://doi.org/10.1364/oe.395185.
30. Lim, K.; Durand, M.; Baudelet, M.; Richardson, M. Transition from Linear-to Nonlinear-Focusing Regime in Filamentation. *Sci. Rep.* **2014**, *4*, 7217. https://doi.org/10.1038/srep07217.
31. Lim, K. Laser Filamentation-beyond Self-Focusing and Plasma Defocusing. Ph.D. Thesis, University of Central Florida, Orlando, FL, USA, 2014.
32. Trojánek, F.; Zídek, K.; Dzurnák, B.; Kozák, M.; Malý, P. Nonlinear Optical Properties of Nanocrystalline Diamond. *Opt. Express* **2010**, *18*, 1349–1357. https://doi.org/10.1364/oe.18.001349.
33. Kudryashov, S.I.; Danilov, P.A.; Smirnov, N.A.; Stsepuro, N.G.; Rupasov, A.E.; Khmelnitskii, R.A.; Oleynichuk, E.A.; Kuzmin, E.V.; Levchenko, A.O.; Gulina, Y.S.; Shelygina, S.N.; et al. Signatures of ultrafast electronic and atomistic dynamics in bulk photoluminescence of CVD and natural diamonds excited by ultrashort laser pulses of variable pulsewidth. *Appl. Surf. Sci.* **2022**, *575*, 151736. https://doi.org/10.1016/j.apsusc.2021.151736
34. Boyd, R.W. *Nonlinear Optics*, 3rd ed.; Academic: Boston, MA, USA, 1992.
35. Jukna, V.; Galinis, J.; Tamosauskas, G.; Majus, D.; Dubietis, A. Infrared extension of femtosecond supercontinuum generated by filamentation in solid-state media. *Appl. Phys. B* **2014**, *116*, 477–483. https://doi.org/10.1007/s00340-013-5723-8.
36. Fang, X.J.; Kobayashi, T. Evolution of a super-broadened spectrum in a filament generated by an ultrashort intense laser pulse in fused silica. *Appl. Phys. B* **2003**, *77*, 167–170. https://doi.org/10.1007/s00340-003-1176-9.
37. Heins, A.; Guo, C. Spectral investigation of higher-order Kerr effects in a tight-focusing geometry. *Opt. Express* **2013**, *21*, 29401–29412. https://doi.org/10.1364/oe.21.029401
38. Kudryashov, S.; Danilov, P.; Smirnov, N.; Levchenko, A.; Kovalev, M.; Gulina, Y.; Kovalchuk, O.; Ionin, A. Femtosecond-laser-excited luminescence of the A-band in natural diamond and its thermal control. *Opt. Mater. Express* **2021**, *11*, 2505–2513 https://doi.org/10.1364/OME.427788
39. Kudryashov, S.I.; Levchenko, A.O.; Danilov, P.A.; Smirnov, N.A.; Ionin, A.A.; IR femtosecond laser micro-filaments in diamond visualized by inter-band UV photoluminescence. *Opt. Lett.* **2020**, *45*, 2026–2029. https://doi.org/10.1364/OL.38934835.
40. Liu, W.; Petit, S.; Becker, A.; Aközbek, N.; Bowden, C.M.; Chin, S.L. Intensity clamping of a femtosecond laser pulse in condensed matter. *Opt. Commun.* **2002**, *202*, 189–197. https://doi.org/10.1016/S0030-4018(01)01698-4
41. Kandidov, V.P.; Fedorov, V.Y.; Tverskoi, O.V.; Kosareva, O.G.; Chin, S.L. Intensity clamping in the filament of femtosecond laser radiation. *Quant. Electron.* **2011**, *41*, 382–386. https://doi.org/10.1070/QE2011v041n04ABEH014486